Hardware-Efficient Programmable-Deviation Controller for Indirect Energy Transfer DC–DC Converters

Mor Mordechai Peretz, *Member, IEEE*, Behzad Mahdavikhah, and Aleksandar Prodić, *Member, IEEE*

***Abstract*—In boost converters and other indirect energy transfer topologies, the fastest transient response usually does not coincide with the minimum possible output voltage deviation. This paper introduces a practical mixed-signal current programmed mode (CPM) controller that, compared to time-optimal solutions, provides a smaller deviation, lower current stress, and simpler controller implementation. To recover from transients, the controller passes through two phases. In the first phase, the inductor current is set in the proximity of its steady-state value, so that the initial transient-caused capacitor charging/discharging process is reversed. In the second phase, the voltage is gradually recovered. The controller implements a simple algorithm for setting up the inductor current and the output voltage peak/valley values during transients, based on the output current estimate, which is obtained through a self-tuning procedure. The operation of the controller is verified both through simulations and experimentally, with a boost-based 12 to 48 V, 100-W prototype, operating at 100-kHz switching frequency. A comparison with a time-optimal controller shows that the introduced programmable-deviation system results in up to 1.9 times smaller voltage deviation while limiting component stress.**

***Index Terms*—Digital control, minimum effort control, minimum energy control, state space methods, switched mode power supplies, time-domain analysis, time optimal control, transient response.**

I. Introduction

To minimize the size of reactive components, the controllers for switch-mode power supplies (SMPS) are often designed to have fast response to load transients and other disturbances. In low-to-medium power supplies, processing power from a fraction of watt to several hundreds of watts, where cost-effective implementation is of a key importance, analog controllers have been predominantly used [1]–[5]. There, a fast response is usually achieved by designing a wide bandwidth control loop.

Recently emerged hardware-efficient digital controllers [6]–[9] enable implementation of advanced nonlinear control methods for low-to-medium power systems, improving dynamic performance and, consequently, drastically reducing the size of the output capacitor. Among them, time-optimal [10]–[19] and minimum-deviation [20] controllers have demonstrated transient response with virtually the smallest possible voltage deviation, for direct energy transfer converters, such as buck and forward topologies. Ideally, in these systems, the load transient response always results in the minimum possible output voltage deviation and, therefore, the minimum output capacitance value. However, for the indirect energy transfer systems, such as a boost converter that is not the case. There, as it will be described in the following section, the time-optimal response often produces a larger than the minimum output voltage deviation, and causes extra current stress of the components. Furthermore, the implementation of the optimal methods for the indirect energy transfer systems is usually more hardware demanding than for the direct energy transfer converters. This is because the controller is required to solve a set of fairly complex operating-point-dependent equations [10], [11], [16], [17]. As a consequence, the previously developed time-optimal controllers still have not been widely adopted in converters with indirect energy transfer.

The main goal of this paper is to introduce a new controller for indirect energy transfer converters that, compared to time-optimal solutions [10]–[18], results in a smaller output voltage deviation allowing for the output capacitor reduction. The controller also reduces current stress of components and has significantly simpler hardware implementation. The programmable-deviation controller of Fig. 1 is primarily designed for converters having output filters with two reactive components (inductor and capacitor) and is a relatively simple modification of a conventional mixed-signal peak current programmed mode (CPM) solution [21]–[26]. Like in the conventional systems, the outer voltage loop is digital and the inner current loop is realized in an analog manner. The voltage loop creates a digital reference for the peak/valley current value $i_{\mathrm{ref}}[n]$ that is then converted into an analog equivalent with a digital-to-analog converter (DAC). During the steady state, the reference is calculated with a PI compensator, based on the error signal of the voltage loop $e_v[n]$, and the resulting output of the DAC is compared to the sensed value of the inductor current $R_s i_L(t)$, with the comparator *i_cmp*. The output of the comparator is then sent to the *S–R* latch and a pulse width modulated (PWM) signal $c(t)$ is created, in the same way as in other CPM solutions [21]–[26].

In this modification, two novel blocks are added. Namely, a *transient suppression block* and a *self-tuning estimator* of the output current are introduced. Upon a load transient detection, these blocks take over the task of creating the PWM

Manuscript received October 14, 2013; revised January 16, 2014 and April 12, 2014; accepted May 23, 2014. Date of publication July 9, 2014; date of current version January 16, 2015. Recommended for publication by Associate Editor T. Geyer.

The authors are with the Laboratory for Power Management and Integrated Switch-Mode Power Supplies, Department of ECE, University of Toronto, Toronto, ON M5S 3G4, Canada (e-mail: morp@ee.bgu.ac.il; bmehrabad@ece.utoronto.ca; prodic@power.ele.utoronto.ca).

Color versions of one or more of the figures in this paper are available online at http://ieeexplore.ieee.org.

Digital Object Identifier 10.1109/TPEL.2014.2332113

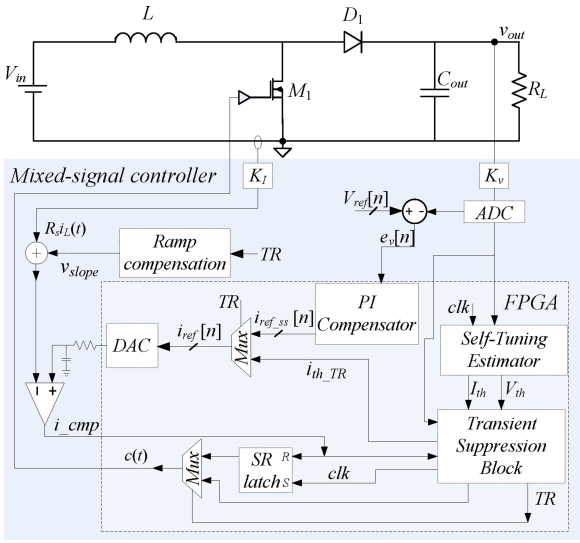

Fig. 1. Programmable-deviation controller regulating operation of a boost converter.

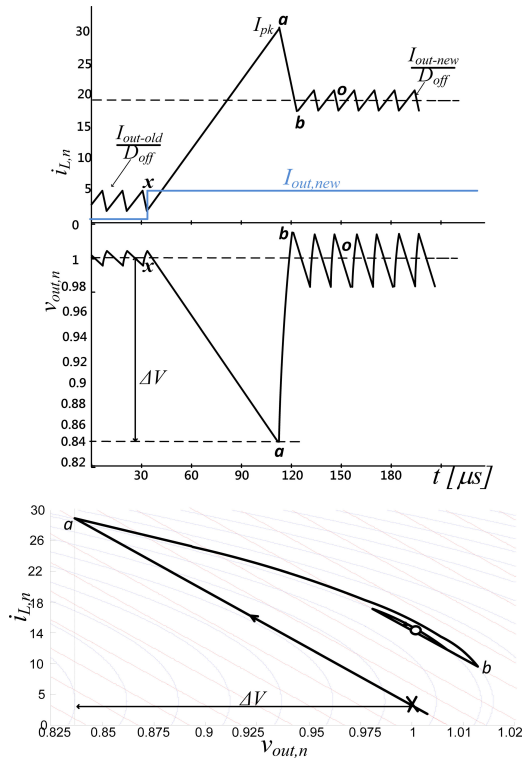

Fig. 2. Operation of an ideal time-optimal controlled boost converter during a light-to-heavy load transient: inductor and load current (top), output voltage (middle), and state-plane representation of the voltage and current (bottom). System parameters are: $V_{\rm in} = 12\,V, V_{\rm out} = 48\,V, I_{\rm load}$—from 1 to 4.5 A.

signal from the conventional controller and provide transient response with near minimum possible voltage deviation. The transient suppression block implements a new transient control algorithm that dynamically changes the on and off transistor times, based on preset values of the peak/valley inductor current and preprogrammed maximum allowable voltage deviation. The estimator's role is to provide the suppression logic with an estimate of the new inductor current, needed for the algorithm. Once the transient recovery is completed, the controller returns to steady-state operation.

II. Transient Mode Controller

The design of the transient mode controller is inspired by the optimum-deviation concept for direct energy transfer converters [20]. There, rather than trying to reduce the output voltage deviation by minimizing the recovery time a more straight-forward approach, directly focusing on the deviation, is taken. In the two-step method presented in [20], the inductor current waveform is first reconstructed to match its new steady-state waveform and, after that, a conventional compensator recovers the voltage. However, due to the much more complex relations between the minimum voltage deviation, inductor, and the load currents, the previously demonstrated method cannot be directly applied for indirect energy transfer converters.

In the programmable-deviation controller introduced in this study, in addition to reconstructing, i.e., programming, the new inductor current value (through output current estimation), the maximum allowable voltage deviation is also programmed. Both of these values are used to obtain near minimum-deviation response while operating the converter over a controlled switching frequency range.

As shown throughout the paper, this design approach brings three main advantages compared to the time-optimal solutions for indirect energy-transfer converters [12]–[18]:

1) the computational complexity is drastically reduced creating a possibility for much simpler, i.e., hardware-efficient, controller implementation;
2) the method results in a significantly smaller output voltage deviation allowing reduction of the output capacitor;
3) the maximum inductor current is lower, approximately equal to its nominal steady-state value, reducing the current stress and allowing for output inductor reduction.

The advantages come from the elimination of complex calculations of the switch ON and OFF times and from the sole reliance on the amplitudes of the state-space variables, which are relatively easy to acquire. Operation of an idealized programmable-deviation controller is explained on a boost converter example, through its comparison with the well-known time-optimal solution [10]–[18]. Figs. 2 and 3 show the load current, inductor current, and the output capacitor voltage during transients, both in the time and the state-plane domains.

In Fig. 2, a typical light-to-heavy response of a time-optimal controlled boost converter is depicted. Fig. 3 shows operation of a near minimum-deviation controlled boost converter. It should be noted that within the scope of this paper and similarly to precursor studies [10]–[18], a constant current or a current step load is assumed. Other load types of load are beyond the scope of the current paper and will be addressed in subsequent publications.

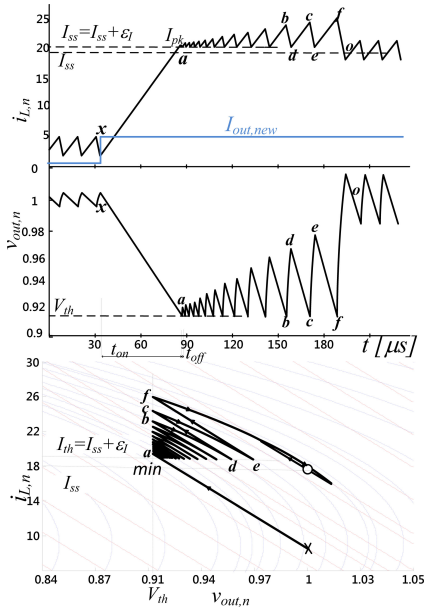

Fig. 3. Operation of a near-minimum-deviation controlled boost converter during a light-to-heavy load transient: inductor and load current (top), output voltage (middle), and state-plane representation of the voltage and current (bottom). System parameters are: $V_{\rm in} = 12\,V$, $V_{\rm out} = 48\,V$, $I_{\rm load}$—from 1 to 4.5 A.

A. Light-to-Heavy Load Transient

The diagrams of Fig. 2 can be used to review operation of the time-optimal controllers and address some of their drawbacks. As soon as a load transient from $I_{\rm out\_old}$ to $I_{\rm out\_new}$ is detected, at point "*x*," the boost converter switch turns ON, causing the inductor current to ramp up with a $V_{\rm in}/L$ slew rate ($V_{\rm in}$ is the input voltage of the converter) and the capacitor voltage to slope down, at $I_{\rm out\_new}/C$ rate. The peak inductor current, $I_{\rm peak1}$, at the time instant *a* is usually significantly larger than its new steady-state value $I_{\rm out\_new}/D_{\rm off}$. Over the following interval, *a* to *b*, when the transistor is turned OFF, this excess of current is used to replace the lost capacitor charge that occurred during the transistor on time. In that way, the fastest possible recovery time to the new steady state is achieved. The problem of the overly large inductor peak current has been addressed in [13] and [18], and several modifications of the optimum-time controller proposed. Those include systems that put a hard limit on the maximum inductor current [13], based on the components rating, and alter the converter configuration with extra switches, to create additional energy paths [18].

From Fig. 2, it can be noticed that, unlike in direct energy transfer converters, for the boost and other indirect energy transfer topologies the time-optimal response does not necessarily result in the minimum output voltage deviation and, therefore, in the minimum output capacitance value. It can be seen that the extra inductor current rise time (beyond its new steady-state value), during which the energy for replacing the lost capacitor charge is collected, increases the current beyond its new nominal value and causes a larger than the minimum possible voltage deviation. This is because the capacitor discharging process continues during the extra time.

To solve this problem, the programmable-deviation controller has been developed. The controller recovers from a transient through a two-step process. Upon detection of a transient, during the first step, the transistor of the boost is turned ON. Over this period, the controller estimates the new load current and accordingly, sets two lower limits, i.e., thresholds, for the output voltage $\rm V_{th}$ and for the inductor current $I_{\rm th}$ such that the minimum inductor current is slightly larger than its new steady-state value $I_{\rm ss}$, (by ε_I), i.e.,

$$I_{\rm th} = I_{\rm ss} + \varepsilon_I. \tag{1}$$

These two values are than used to determine the switching sequence upon the initial turn ON of the transistor, i.e., the switching sequence for the second phase of the recovery from the transient. The voltage threshold value is calculated such that, for a given frequency operation range, the output voltage deviation is minimum. The current threshold is set such that it ensures that the converter recovers to steady state by following a stable convergence trajectory [27]–[34]. As demonstrated in [28], [30], and [32], the inductor threshold value given by (1) results in stable convergence toward the new steady-state value with a near-minimum possible voltage deviation.

During the recovery phase, the transistor on time is controlled by the voltage threshold reference and its off time by the current threshold value. By comparing Figs. 2 and 3, it can be seen that at the expense of slightly slower recovery time, several advantages of this implementation are achieved over time-optimal solution. Namely, due to a shorter period in which the capacitor is discharged, lower output voltage deviation ΔV and current stress are obtained. Also, as will be shown in the following section, the computational demands are significantly reduced. This is because the calculation of the switch transition point values (labeled as *a* to *e* in Fig. 3) is much simpler than the calculation of the point *a* for the time-optimal case (see Fig. 2), which usually involves solving a set of nonlinear operating condition-dependent equations [13], [16], [17]. The advantage can also be understood through recognizing that the programmable-deviation controller eliminates the need to accurately calculate transistors on and off times, which are explicit parameters, and deals with the amplitudes of the signals that can be measured relatively easy.

It can also be observed from Fig. 3 that the minimum voltage deviation ("min," Fig. 3) occurs when the converter operates such that the slope of the first on state matches the local slope, i.e., derivative, of an off state on the state plane. As pointed out in [28] and demonstrated in [30]–[34], this location is also the intersection point of the first "on" state trajectory and the load line (value of the new steady-state current—minimal current threshold). However, convergence to the steady state (point "0") from this point would require operation at a very high switching frequency (theoretically infinite for the case when $V_{\rm th}$ is equal to the minimum deviation) and, as such, is not practical. Therefore, $V_{\rm th}$ is set to be slightly lower than the minimum voltage deviation and the switching frequency range is limited. As an example, Fig. 4 shows simulation results for the case when $V_{\rm th}$ is set to be a 4% lower than the minimum possible deviation and the switching frequency is limited to a practical value.

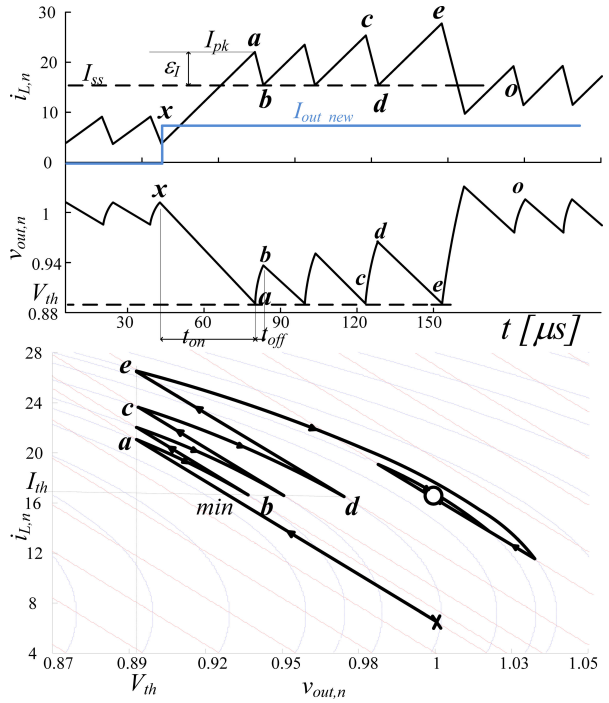

Fig. 4. Operation of the programmable-deviation controller in a boost converter for light-to-heavy load transient (maximum switching frequency is limited). Inductor and load current (top), output voltage (middle), and state-plane representation of the voltage and current (bottom). System parameters are: $V_{\rm in} = 12\,V$, $V_{\rm out} = 48\,V$, $I_{\rm load}$—from 1 to 4.5 A.

Another aspect of comparison and superiority of the programmable-deviation controller over the time-optimal approach is the issue of switching losses during a transient event. Considering the somewhat longer transient recovery period of the programmable-deviation control as a time frame for comparison, it can be observed that the introduced method has fewer switching actions (see Fig. 4) than the time-optimal one (see Fig. 2). This is because the switching sequence governed by the suppression logic (comparator action) operates at a lower switching rate than the steady-state switching rate, which in the case of the time-optimal solution resumed earlier. In addition, the programmable-deviation controller operates with lower peak current that allows selection of smaller power switches with lower parasitic capacitances. As a consequence, the following benefits, in the context of switching losses, are obtained: 1) lower peak current, 2) power switches with smaller parasitic capacitance, and 3) fewer switching actions over the voltage recovery period. It should also be noted and can be observed from Figs. 2–4 that the amount of switching actions per a transient event is inversely proportional to the voltage threshold that is selected, i.e., larger deviation requires less transitions toward the stead state. As aforementioned, the ideal case of minimum deviation (see Fig. 3) would result in infinite switching actions at infinite frequency, and hence would introduce higher switching losses. This issue further highlights the motivation for the development of the programmable-deviation (see Fig. 4) controller that by the flexibility in the selection of the voltage deviation limits the switching frequency to a finite and practical value.

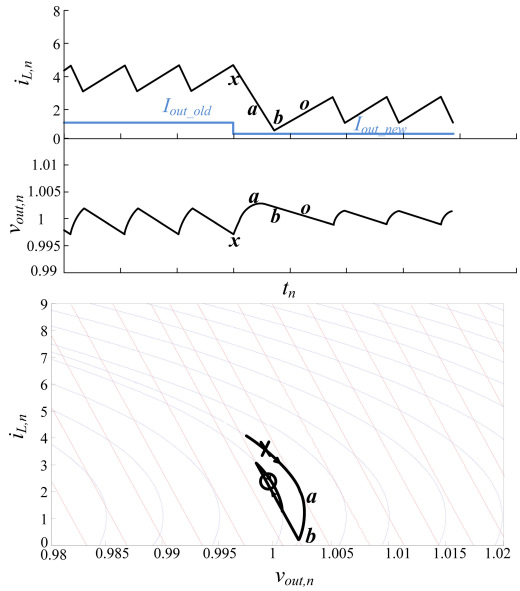

Fig. 5. Operation of the programmable-deviation controller in a boost converter for heavy-to-light load transient. Inductor and load current (top), output voltage (middle), and state-plane representation of the voltage and current (bottom). System parameters are: $V_{\rm in} = 12\,V$, $V_{\rm out} = 48\,V$, $I_{\rm load}$—from 1 to 0.5 A.

B. Heavy-to-Light Transients

For heavy-to-light transitions (see Fig. 5), the operation is similar to the time-optimal control [10]–[18]. The transistor is turned OFF until the output voltage recovers from the initial overshoot and goes back to its steady-state value. Thereafter, the steady state, i.e., PI, mode of controller operation is resumed with the initial inductor current reference set to be equal to the estimated steady-state value.

It can be observed from Fig. 5 that the recovery from heavy-to-light transient starts with turning the transistor OFF until the inductor current is smaller than the new load value. In state space, it corresponds to the state point where the trajectory slope changes from negative to positive (point "*a*," Fig. 5). This point is the absolute minimum deviation [28], [30]. Turning the transistor ON before this point would result in a larger overshoot, longer transient, and a possible runaway situation [27] (i.e., the output voltage continues to increase). Once this point is reached, various switching sequences can be created to recover the converter to the new steady state. The recovery can be done in small increments similar to the light-to-heavy case or, as implemented here, by keeping the transistor OFF until the output voltage reaches the steady-state value (point "o," Fig. 5). The latter has been adopted in this case because it involves fewer transitions and, therefore, is faster and requires less computing resources.

III. Light-to-Heavy Transition Thresholds Derivation

The thresholds of the output voltage and inductor current during a light-to-heavy load transient are selected such that the voltage deviation due to the transient is minimized and, at the

same time, the converter has sufficient energy to converge to the new operating point. That is, the inductor current has to be larger than its new steady-state value, to restore the charge balance of the output capacitor. An explanation of this conjecture can be found from the state trajectories of Fig. 4. They show that to facilitate a trend of voltage increments toward the steady-state point "*0,*" from a starting point "*x,*" the initial on time must be long enough to ensure that the following off time starts at a point where the inductor current is higher than the current of the next on time. In Fig. 4, those two points are labeled as *a* and *b*, respectively. From the state-space point of view, this means that the inductor current must climb up the on-trajectory to a point where the slope of the trajectory is equal or greater than the slope of an intersecting off-trajectory (point "min," Fig. 4). This will be guaranteed when the on time starts with the inductor current larger than its new steady-state value.

To find the boundary values, several approaches can be taken. For example, derivation of the minimum deviation loci out of the state-space equations has been presented in [28]. Although it has many merits, in terms of theoretical methodology and proof of stability (which is beyond the scope of this paper and will be addressed in detail in subsequent publications), the time parameter is implicit. As a result, an implementation of a controller with controllable switching frequency would be very challenging, and, due to the associated computational burden, probably impractical in a number of applications.

In this study, the effect of a full on-off cycle on a boost converter is considered to derive the boundary values. For the following derivations, it is assumed that all the components are ideal and that the new value of the load current step is known. It should be noted that without losing generality, the parameters $t_{\rm on}$ and $t_{\rm off}$ used throughout the derivations refer to the conduction time M_1 switch (see Fig. 1) and may be different than their steady-state values.

The voltage drop during the on time can be expressed as follows:

$$V_{\rm th} = V_{\rm out} e^{-\frac{t_{\rm on}}{\tau}} \tag{2}$$

where $V_{\rm th}$ is the maximum allowed output voltage deviation during load transient, $V_{\rm out}$ is the steady-state output voltage, and $\tau = R_L C_{\rm out}$, where $R_L = V_{\rm out}/I_{\rm out\_new}$ is the new equivalent load resistance and $C_{\rm out}$ is the output capacitance.

The peak inductor current at the end of the on state is found to be

$$I_{pk} = \frac{I_{\rm out\_old}}{D'_{\rm oss}} + \frac{V_{\rm in}}{L} t_{\rm on} \tag{3}$$

where $I_{\rm out\_old}$ is the previous value of steady-state load current, just before the load transient has occurred, $D_{\rm oss}$ represents the M_1 switch "on" duty ratio during steady-state operation and $D'_{\rm oss} = 1 - D_{\rm oss}$.

Based on the condition for positive increment set earlier in (see 1), the inductor current at the beginning of the off state must satisfy

$$I_{pk} - \varepsilon_I = \frac{I_{\rm out\_new}}{D'_{\rm oss}}. \tag{4}$$

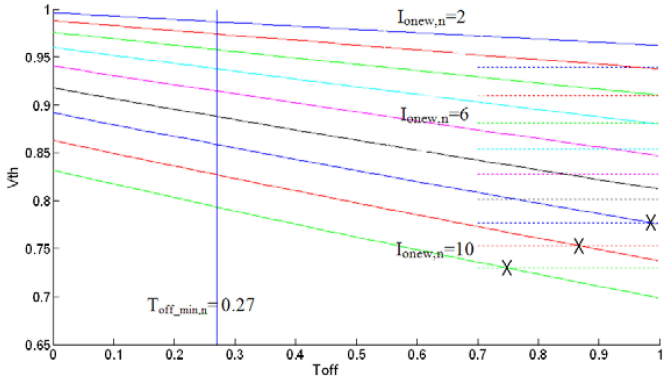

Fig. 6. Normalized curves of minimum $V_{\rm th}$ versus allowed $t_{\rm off}$ for different load steps ranging from $2I_{\rm ref}$ to $10I_{\rm ref.}$. The blue vertical line shows limitation on $V_{\rm th}$ by maximum switching frequency and the cross marks show points limited by the peak current.

During the off state, the inductor current is allowed to ramp from I_{pk} down to $I_{\rm out\_new}/D'_{\rm oss}$ ($t_{\rm off}$ in Fig. 4). To establish the relationship to the timing parameter $t_{\rm off}$, the value of ε_I as a function of the converter parameters during the off state can be expressed as follows:

$$I_{pk} - \frac{I_{\rm out\_new}}{D'_{\rm oss}} = \varepsilon_I = \frac{V_{\rm out} - V_{\rm in}}{L} t_{\rm off}. \tag{5}$$

Substituting (5) into (4) yields the condition for inductor current at the beginning of the off state, that is

$$I_{pk} - \frac{V_{\rm out} - V_{\rm in}}{L} t_{\rm off} = \frac{I_{\rm out\_new}}{D'_{\rm oss}}. \tag{6}$$

Combining (2), (3), and (6) and after some manipulations the minimum threshold voltage as a function of the off time is found to be

$$V_{\rm th} = V_{\rm out} e^{-\left[\frac{\frac{I_{\rm out\_new} - I_{\rm out\_old}}{D'_{\rm oss}} + \overbrace{\frac{V_{\rm out} - V_{\rm in}}{L} t_{\rm off}}^{\varepsilon_I}}{\frac{V_{\rm in}}{L}\frac{V_{\rm out}}{I_{\rm out\_new}} C_{\rm out}}\right]}. \tag{7}$$

It should be noted that the criterion set by (7) guarantees that the inductor current value at the beginning of the off state (e.g., point "*e*" in Fig. 4) will be higher than the peak inductor current of the previous on state (e.g., point "*c*" in Fig. 4). That is, it assures the recovery (increment) of the inductor toward the steady state. It should also be noted that although stability analysis of the method is beyond the scope of this study (will be detailed in subsequent publications), the fact that the voltage threshold criterion of (7) is based on that the inductor current has satisfied (1), i.e., reached a value beyond the load line, comes in agreement with the stability analyses discussed in [31]–[34] and with the energetic balance theory presented in [30].

Fig. 6 shows normalized curves of (7) for different load step values. The normalization is obtained through the following

relationships [10], [11]:

$$V_n = \frac{V}{V_{\rm ref}}\,,\; I_n = \frac{I}{I_{\rm ref}}\,,\; t_n = \frac{t}{T_{\rm ref}}\,,\; L_n = \left(\frac{I_{\rm ref}}{V_{\rm ref}t_{\rm ref}}\right)L\,,\; C_n = \left(\frac{V_{\rm ref}}{I_{\rm ref}t_{\rm ref}}\right)C \tag{8}$$

where the base values $V_{\rm ref}$ and $I_{\rm ref}$ are assigned as the steady-state output voltage and the previous value of steady-state load current $I_{\rm out\_old}$, respectively, $T_{\rm ref} = \sqrt{\rm LC}$.

Given finite minimal off time value $t_{\rm off} = T_{\rm off\_min}$, based on the maximum switching frequency that is allowed by the controller, the minimal voltage deviation that can be achieved can be expressed as follows:

$$V_{\rm th}\,|_{t_{\rm off}=T_{\rm off\_min}} = V_{\rm out}e^{-\left[\frac{\frac{I_{\rm out\_new}-I_{\rm out\_old}}{D'_{\rm oss}}+\frac{V_{\rm out}-V_{\rm in}}{L}T_{\rm off\_min}}{\frac{V_{\rm in}}{L}\frac{V_{\rm out}}{I_{\rm out\_new}}C_{\rm out}}\right]}. \tag{9}$$

In case that a peak inductor current limit is required, the resultant voltage deviation can be expressed as follows:

$$V_{{\rm th},n} = V_{{\rm out},n}e^{-\left[\frac{I_{pk,n}-\frac{I_{\rm out\_old},n}{D'_{\rm oss}}}{\frac{V_{{\rm in},n}}{L_n}\frac{V_{{\rm out},n}}{I_{{\rm out\_new},n}}C_{{\rm out},n}}\right]} \tag{10}$$

where $T_{\rm off\_min}$ is the minimum allowed off time $I_{pk,n} = I_{\rm limit} + \varepsilon_I$, and $I_{\rm limit}$ is the normalized maximum allowed switch current.

The boundary values of $V_{\rm th}$ in terms of maximum frequency (minimum $t_{\rm off}$) and the maximum inductor current are delineated in Fig. 6. From the window created by the boundaries of $(T_{\rm off,min}, V_{\rm th})$, a map of current and voltage limits is constructed for the entire load range. As it will be shown in the following section, this map is then used for look-up table (LUT) based practical implementation of the controller. Fig. 6 also shows that, as opposed to buck converter [12]–[19], the mechanism to obtain minimum voltage drop in a boost converter is not unique (until the valley point) and strongly depends on the load conditions and frequency limitations of the controller.

By manipulating (7), the additional charging current over the steady-state point ε_I can be expressed as a function of the voltage threshold and the system parameters are as follows:

$$\varepsilon_I = \frac{V_{\rm in}^2}{D'_{\rm oss}I_{\rm out\_new}}\frac{C_{\rm out}}{L}\ln\left(\frac{V_{\rm out}}{V_{\rm th}}\right) - \frac{I_{\rm out\_new}-I_{\rm out\_old}}{D'_{\rm oss}}. \tag{11}$$

Given the information of the load current, system parameters, and the desired voltage deviation, the initial charging current can be calculated using (11). To reduce the sensitivity of the threshold voltage estimation on the system parameters, estimation of the system components can be applied. An output capacitance estimation method has been developed and is described in the following section. Reliable estimation of the inductance value can be obtained using the method developed in [21]. Furthermore, the result of (11) lays out the foundations to an alternative, more robust, programmable-deviation control scheme that realizes the initial charging phase based on the inductor current, rather than on the output voltage and, therefore, is less dependent of the converter parameters. The algorithm and additional results are briefly delineated in Appendix A.

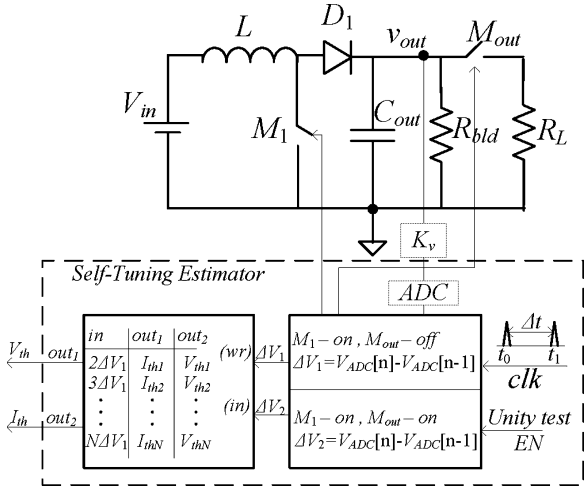

Fig. 7. Block diagram of the self-tuning estimator.

IV. Practical Implementation

The time-optimal control solutions for the boost converter [10], [11], [16], [17] usually require continuous and fast sampling, i.e., oversampling, of the both state variables. They also require fairly demanding calculations, to determine the converter operating point (its location on the state space) and create the switching sequence. The programmable-deviation controller operates with a much simpler algorithm and can be implemented by sampling the output voltage at the switching frequency rate, i.e., without oversampling. As shown in Fig. 1, the controller is a modification of a simple mixed-signal peak CPM controller, where the *self-calibration block* and *transient suppression logic* are added. As described later, the self-calibration logic is used to determine the voltage and current threshold values, $V_{\rm th}$ and $I_{\rm th}$, described in Section III. These two values are then passed to the transient suppression logic that creates the switching sequence.

A. Self-Tuning Estimation and Transient Suppression Logic

The implementation of the self-tuning estimator of Fig. 7 is based on a LUT and on the estimation of the load current (and from it, steady-state inductor current) through a comparison with a measurement of the known current value, named the unity current. The LUT of the estimator is populated during the converter start up. Over that period, the LUT's entries are stored, i.e., current and voltage threshold values are created, from the measurement of the output capacitor voltage derivative during the on-time of the switch M_1. After the writing of the values in the tables is completed, the voltage deviation of the capacitor is used as an address (input *in* of Fig. 7) to determining LUT outputs, i.e., $V_{\rm th}$ and $I_{\rm th}$ values.

The process of the output load estimation is described with Figs. 7–9. Upon the converter power up, a generic LUT based on the calculation of (9) (or with a simplified expression as

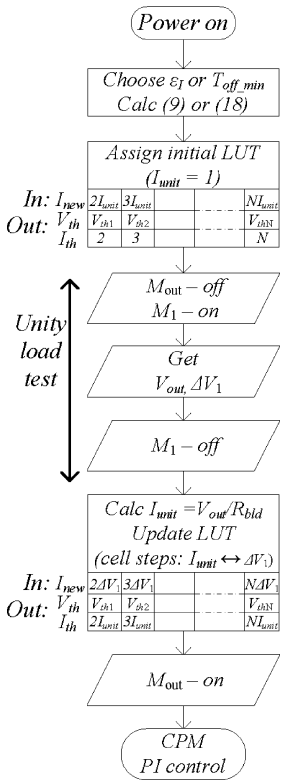

Fig. 8. Flowchart of the unity load test and the LUT population procedure.

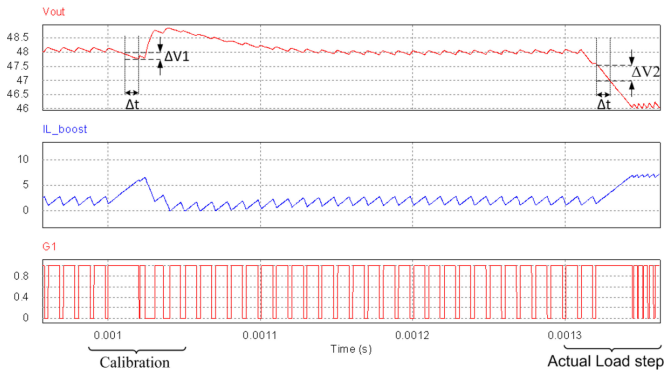

Fig. 9. Calibration process for load and inductor current, followed by a light-to-heavy load transient.

will be shown later in this section) is assigned (see Fig. 8). The known current of the protective resistor $R_{\rm bld}$ (also known as bleeding resistor), named unit current $I_{\rm unit}$, is used for the system calibration and for updating the LUT to comply with the measured values in the system. During this time, the load is disconnected from the output of the converter, i.e., switch $M_{\rm out}$ is turned OFF, and the value ΔV_1, proportional to the unit current $I_{\rm unit}$, is measured as follows:

$$\Delta V_1 = v_{\rm adc}[n] - v_{\rm adc}[n-1] = \frac{V_{\rm ref}}{R_{\rm bld}}\frac{\Delta t}{C} = I_{\rm unit}\frac{\Delta t}{C} \quad (12)$$

where Δt is the sampling interval, $v_{\rm adc}[n]$ is the current value of the analog-to-digital converter (ADC) output and $v_{\rm adc}[n-1]$ is the ADC value from the previous sampling cycle. The value ΔV_1 is used to populate the LUT with $I_{\rm th}$ and $V_{\rm th}$ values for the full range of allowable output voltage deviations, i.e., for the initial write process. It can be seen that the value ΔV_1 uniquely determines the relation between the capacitor voltage deviation and the load currents and, therefore, $I_{\rm th}$ values. As shown in Figs. 7 and 8, the threshold values of the inductor current are written in the table as scaled steps of the measured unit current value. This implies that once the LUT has been populated, $V_{\rm th}$ and $I_{\rm th}$ values will be determined based on the new load current only, which eliminates the dependency of the controller on the information of the previous loading conditions (i.e., $I_{\rm out\_old}$). For slow and/or light load transients, i.e., smaller than the quantization steps of the current estimator, the output voltage variations are relatively small and the transient logic is not activated. For those cases, the conventional PID compensator of Fig. 1 is sufficiently fast to perform regulation of the output voltage and keep the output voltage deviation under the maximum allowable value.

The unity load test also allows for the identification of the output capacitance and subsequent population of the LUT with $V_{\rm th}$ values (based on the output voltage measurement), in accordance with (9) or (18). It should be noted that in the table population process it is assumed that the information about D', needed for the calculations of both set of table entries, is known. The value of D' can be extracted from the feedback loop using a fairly simple counter [20].

Once the power up of the converter and population of the LUT are completed, the switch $M_{\rm out}$, usually existing in the applications of interest, is turned ON. During the remaining portion of the converter operation, the LUT is used to produce $I_{\rm th}$ and $V_{\rm th}$ during transient events. As shown in Fig. 7, the input to the table is now the voltage deviation ΔV_2 measured during the on time of the main switch M_1. During a transient event, the load current $i_{\rm out\_new,n}$ is estimated as follows:

$$\frac{\Delta V_2}{\Delta V_1} = \frac{I_{\rm new} + I_{\rm unit}}{I_{\rm unit}} = i_{\rm out\_new,n} \quad (13)$$

and the corresponding values of the threshold current and the voltage are produced by the LUT. These values are than passed to the transient suppression logic that suppresses the output voltage deviation by applying the switching sequence described in Section II and depicted with the flowchart diagram of Fig. 10.

The comparison of the successive output voltage samples is also used for transient detection in a similar manner to the one presented in [35] and [36]. Such sampling introduces a maximum delay in a transient detection equal to one sampling period. For the cases when the delay caused by this detection method is not acceptable, a simple dedicated transient detection circuit, similar to the solution present in [20] can be used.

It should be noted that due to the mixed-signal implementation, the inductor current ripple does not affect the proper operation of this controller. This is because the new reference current value, which was calculated based on the estimated load transient, is compared to the instantaneous current of the inductor and the information about the average inductor current is not needed. Still, it should be pointed out that the time needed for the inductor current to reach the new reference (and

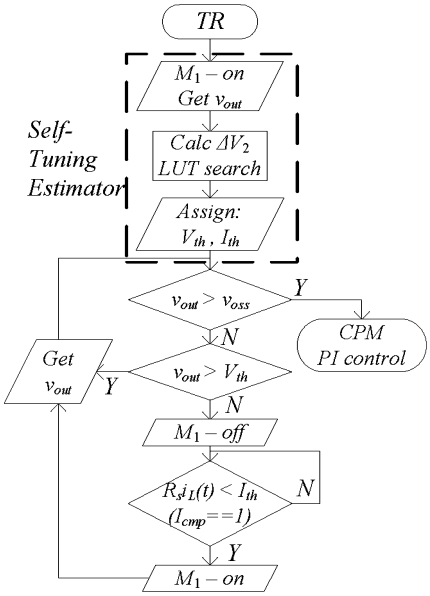

Fig. 10. Flowchart of the transient suppression algorithm. ($v_{\rm oss}$ is the output voltage steady-state value)

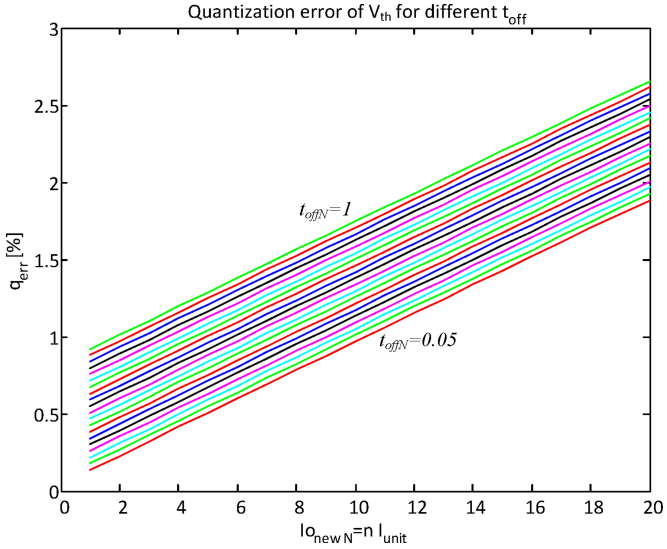

Fig. 11. Quantization error of the threshold voltage LUT value as a function of the load conditions for the entire $t_{\rm off}$ range. Calculation is based on LUT density of $I_{\rm unit} = I_{\rm nominal}/20$.

therefore the recovery time) depends on the instantaneous inductor current at the time instant of the transient. This means that for the converters with larger current ripple that time could vary significantly. In Section IV B, the effect of the fixed sampling rate on the accuracy of the voltage deviation is addressed and quantified.

Based on the unity load test, the output capacitor can be estimated by

$$\frac{1}{C} = \frac{R_{\rm bld}}{V_{\rm out}} \frac{\Delta V_1}{\Delta t} \tag{14}$$

where Δt is the time duration that results in ΔV_1 drop in output voltage as shown in Fig. 9. It should be noted that the value $1/C$ (rather than C itself) is the parameter of interest for the calculations in (7), (9), and (12).

B. Nonideal System

The effect of the equivalent series resistance (ESR) on the voltage threshold is dependent on the load change and given the ESR, its effect may be added as a constant for each $V_{\rm th}$ curve on Fig. 6, that is

$$V_{\rm th+ESR} = V_{\rm th} + I_{\rm new}{\rm ESR}. \tag{15}$$

A relatively slow sampling rate may cause delayed transient detection, and as a result a delay in turning the transistor ON and increased voltage drop. As a consequence, an error in the voltage threshold detection could occur. This effect is dependent on the load value and the sampling rate.

The worst case would be that the sampling is delayed by one sampling cycle (switching period). The additional voltage drop $V_{\rm dly}$ can be expressed as follows:

$$V_{\rm dly} = \frac{I_{\rm new} T_s}{C} \tag{16}$$

where T_s is the sampling period. $I_{\rm new}$ and C can be estimated by the aforesaid procedure.

A possible solution for this problem would be to base the voltage sensing circuitry on a comparator such as in [20] and/or increase the sampling rate. However, as it will be experimentally shown in the following section, even a relatively low sampling rate, at the switching frequency of the converter, provides good transient response of the introduced controller. As described in [20], this is mostly due to a low susceptibility of the minimum deviation method on the system delays and quantization effects.

C. LUT Quantization Error and Computing Effort

As described by Fig. 7, the voltage deviation ΔV_2 is used to pick up the threshold values form the LUT. The discrete nature of the table may result in quantization error that, in turn, may impact the performance of the transient recovery. The amount of deviation from the desired threshold value primarily depends on the density of the table, i.e., on the unity load current which determines the table density. The quantization error $q_{\rm err}$ per two neighboring cells of the LUT ($V_{\rm th}[n], V_{\rm th}[n+1]$) can be expressed as follows:

$$q_{\rm err} = \frac{V_{{\rm th}[n]} - V_{{\rm th}[n+1]}}{V_{{\rm th}[n]}} \tag{17}$$

where the index n represents the cell location that corresponds to $I_{\rm out\_new} = nI_{\rm unit}$.

Fig. 11 plots the expected quantization error of the normalized $V_{\rm th}$ of Fig. 6 as a function of the load current for various cases of ε_I. The unity load value is selected to be 1/20 of the nominal current. It can be observed that even with modest spacing of the LUT, the maximum error from the desired value is in the range of 2%.

The realization of (9) and the population of the LUT, although carried out once during the startup of the system, requires significant amount of computing resources that may not be available

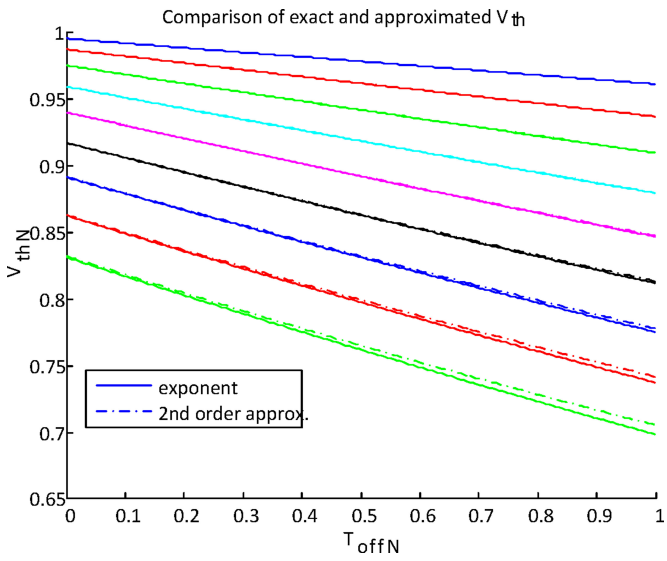

Fig. 12. Comparison of exponent-based—(9) (solid lines), and approximation-based—(18) (dot-dashed lines) extraction of the threshold voltage map.

in low-cost microcontrollers. However, it has been found that the simple second order Taylor expansion of the exponent in (9), i.e., $e^{-x} = 1 - x + x^2/2$, is in a very good agreement with the original expression for the entire operation range. Applying this manipulation, the exponential equation in (9) can be approximated to

$$V_{\rm th} \approx V_{\rm out}\left(a{I_{\rm out\_new}}^4 + b{I_{\rm out\_new}}^3 + c{I_{\rm out\_new}}^2 + dI_{\rm out\_new} + 1\right) \quad (18)$$

$$a = \frac{K_1^2}{2}, b = K_1K_2, c = \frac{K_2^2}{2} - K_1, d = -K_2$$

where

$$K_1 = \frac{L}{D'_{\rm oss}V_{\rm in}V_{\rm out}C}$$

$$K_2 = -\frac{I_{\rm out\_old}L}{D'_{\rm oss}V_{\rm in}V_{\rm out}C} + \frac{V_{\rm out} - V_{\rm in}}{V_{\rm in}V_{\rm out}C}t_{\rm off}.$$

This implies that a simplified polynomial expression that depends on the new load current as a parameter, and other known constants of the system can be used to solve (9) with reduced computational effort. Fig. 12 redraws Fig. 6 for comparison of the original expression (9) and the approximated expression (18) of $V_{\rm th}$. As can be observed, the results coincide with negligibly small discrepancy in the range of 1%.

Substituting (13) into (18) enables a direct extraction of the threshold value based on the voltage deviation ratio ($\Delta V_2 \Delta V_1 = I_{\rm out\_new}$), i.e., load current measurement

$$V_{\rm th} \approx V_{\rm out}\left(a\left(\frac{\Delta V_2}{\Delta V_1}\right)^4 + b\left(\frac{\Delta V_2}{\Delta V_1}\right)^3 + c\left(\frac{\Delta V_2}{\Delta V_1}\right)^2 + d\left(\frac{\Delta V_2}{\Delta V_1}\right) + 1\right) \quad (19)$$

which allows further reduction of the computational effort from the controller.

As can be observed from (18) and mentioned earlier in Section III, a reliable estimation of the threshold voltage depends on the information of the system parameters, which are prone to vary over time, temperature or stress. To enhance the reliability of the estimation, output capacitance estimation procedure based on the unity load test, as described in (14), can be applied. Inductance value estimation can be obtained as prescribed in [21]. To further enhance the reliability of the method, an alternative threshold setup approach based on only the load current has been carried out and is described in Appendix A.

V. Experimental Verification

To verify the effectiveness of the introduced programmable-deviation control method, an experimental prototype was built based on the diagrams shown in Figs. 1, 7–9. The 12 V–48 V, 100-W boost converter operates at a switching frequency of 100 kHz. The digital controller implementing PI steady-state control law and the new transient recovery algorithm was implemented with an field-programmable gate array-based prototype [37] and readily available ADC converters. The entire controller realization (CPM and the programmable deviation) requires only 9000 logic elements allowing its implementation with only a 20% of resources of a low-cost FPGA system such as [38], whose price is comparable or even lower than that of simple microcontrollers widely used in the industry, e.g., [39], [40].

The performance of the controller was tested for the voltage sampling rate equal to the switching frequency and for the case when the output voltage was over sampled at a 32 × sampling rate. The performances of the introduced controller were also compared to that of a state of the art time-optimal solution, which was built following the implementation demonstrated in [13], [16] and [17]. Also, comparisons with a conventional mixed-signal peak current programmed mode controller [21]–[25] (PCPM), requiring much simpler implementation than that of the time-optimal solutions were performed.

Figs. 13 and 14 show a comparison of the transient responses of the time-optimal solution and the introduced programmable-deviation controller for a light-to-heavy load transient. In both the cases, the output voltage was sampled 32 times. It can be seen that the output voltage deviation for the programmable-deviation controller is about 1.9 times smaller than that of the time-optimal system and that the current stress is reduced by 1.3 times. These results show that the programmable-deviation controller allows for the use of significantly smaller output capacitance value (about 1.9 smaller), switching components with 1.3 times lower peak current ratings and an inductor with about 1.69 times smaller maximum energy storage capacity, which is proportional to the squared value of the peak inductor current.

Fig. 15 shows comparisons of the transient responses of the conventional PCPM controller [21]–[26] requiring one voltage sample per a switching period with that of the programmable-deviation solution for two cases: 1) when the sampling is performed once per switching cycle and 2) when a 32 × sampling

Fig. 13. Light-to-heavy load transient response (12.5 W–75 W) of the time-optimal controller with 32× sampling rate. Ch.1 (upper trace): the ac component of the output voltage, 2 V/div; Ch.2 (bottom trace): inductor current, 5 A/div. The time scale is 50 μs/div. Operating conditions: $V_{\rm in} = 12\,V, V_{\rm out} = 48\,V, L = 50\,\mu$H, and $C_{\rm out} = 25\,\mu F$.

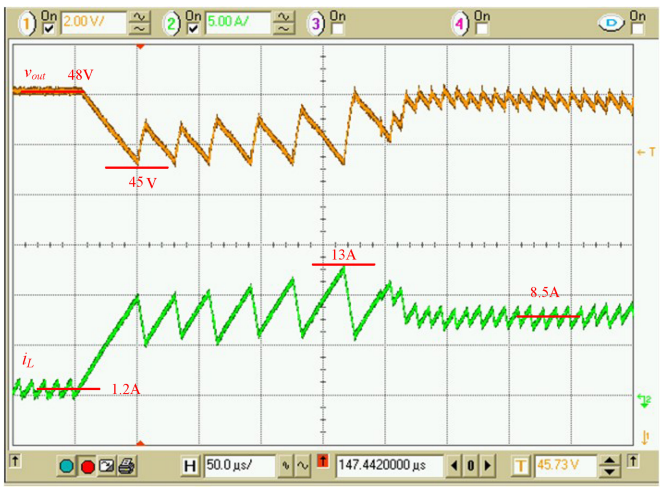

Fig. 14. Light-to-heavy load transient response (12.5 W–75 W) of the programmable-deviation controller with 32 × sampling rate. Ch.1 (upper trace): the ac component of the output voltage, 2 V/div; Ch.2 (bottom trace): inductor current, 5 A/div. The time scale is 50 μs/div. Operating conditions: $V_{\rm in} = 12\,V, V_{\rm out} = 48\,V, L = 50\,\mu H$, and $C_{\rm out} = 25\,\mu F$.

rate is applied. The PCPM controller is regulated with a fast loop having the bandwidth of approximately one-tenth of the switching frequency. It can be seen that in both the cases the transient response is drastically improved. By comparing the responses of the programmable-deviation controller for once per cycle and 32 × sampling rates, we can see that a drastic reduction in the sampling rate has a minor effect on the transient performance, allowing for a simple ADC to be used. Results confirm discussion from Section IV B and also demonstrate that, even with much lower sampling rate, the performance of the programmable-deviation controller is significantly better than that of time-optimal solution (shown in Fig. 14).

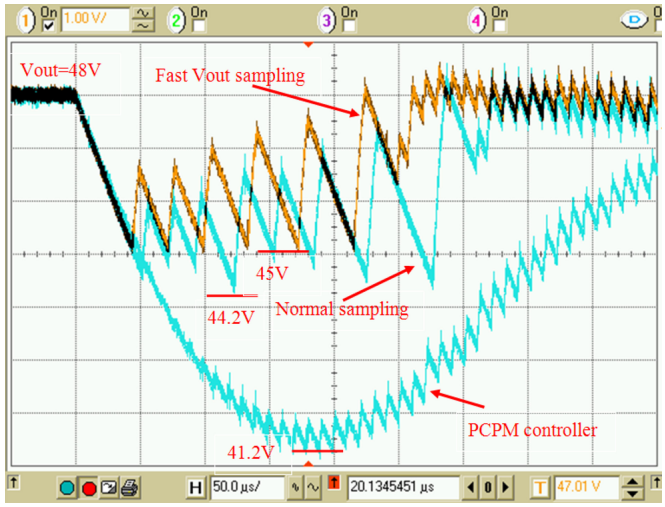

Fig. 15. A comparison of the light-to-heavy load transient response (12.5 W–75 W) of the conventional PCPM controller and the programmable-deviation controller for: (a) once per switching cycle sampling rate and (b) 32 × sampling rate. AC components of the output voltage, 2 V/div. The time scale is 50 μs/div. Operating conditions: $V_{\rm in} = 12\,V, V_{\rm out} = 48\,V, L = 50\,\mu$H, and $C_{\rm out} = 25\,\mu$F.

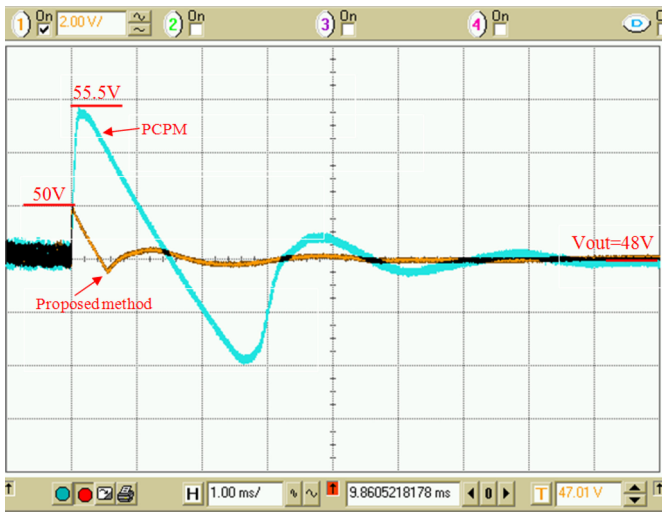

Fig. 16. A comparison of the heavy-to-light load transient response (75 W–12.5 W) of the conventional PCPM controller and the programmable-deviation controller for once per switching cycle output voltage sampling rates; AC components of the output voltages, 2 V/div. The time scale is 1 ms/div. Operating conditions: $V_{\rm in} = 12\,V, V_{\rm out} = 48\,V, L = 50\,\mu$H, and $C_{\rm out} = 25\,\mu$F.

Fig. 16 shows a comparison of transient responses of the programmable-deviation and PCMP controllers for heavy-to-light load transients for the case when the both controllers sample the output voltage once per switching cycle. It can be seen that for the new controller, the deviation is about 3.7 times smaller, allowing for the same reduction of the output capacitor value. The results confirm that this, relatively small, modification of the conventional CPM architecture drastically improves the transient performance allowing for a significant reduction of the reactive components.

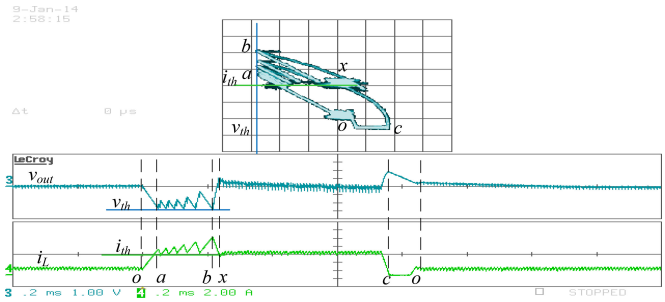

Fig. 17. Light-to-heavy–heavy-to-light load transient response (25 W–90 W–25 W) of the programmable-deviation controller with its corresponding state trajectories. Upper plot: *XY* plot (*X*—output voltage, *Y*—inductor current). Lower plot: Ch.3 (upper trace): the ac component of the output voltage, 1 V/div; Ch.4 (bottom trace): inductor current, 2 A/div. The time scale is 200 μs/div. Operating conditions: $V_{\rm in} = 12\,V, V_{\rm out} = 48\,V, L = 100\,\mu$H, and $C_{\rm out} = 25\,\mu$F.

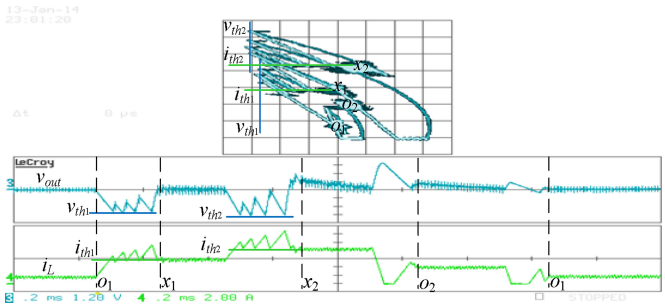

Fig. 18. Tight voltage regulation of the programmable-deviation controller for two consecutive load transients (25 W–90 W–140 W–75 W–25 W) with the corresponding state trajectories. Upper plot: *XY* plot (*X*—output voltage, *Y*—inductor current). Lower plot: Ch.3 (upper trace): the ac component of the output voltage, 1.2 V/div; Ch.4 (bottom trace): inductor current, 2 A/div. The time scale is 200 μs/div. Operating conditions: $V_{\rm in} = 12\,V, V_{\rm out} = 48\,V, L = 100\,\mu$H, and $C_{\rm out} = 25\,\mu$F.

Another set of experiments has been carried out to validate the concept with respect to the state-plane theory described in Section III and to verify the robustness of the method for consecutive load transients. Fig. 17 shows a light-to-heavy and a heavy-to-light load transient in a single frame with their state trajectory plot. Fig. 18 shows the operation of the programmable-deviation controller for two consecutive load steps, demonstrating tight voltage regulation. It should be noted that the load step results presented in Fig. 18 have been implemented with a modified algorithm for the threshold selection, as described in Appendix A.

VI. Conclusion

The hardware-efficient programmable-deviation controller for indirect energy transfer converters introduced in this paper is a modification of the conventional mixed-signal PCPM architecture. The controller is designed around the fact that, for indirect energy transfer converters, the time-optimal response does not coincide with the minimum possible voltage deviation. Therefore, it is designed with the goal of providing near minimum possible voltage deviation for a controlled switching frequency operating range. Compared to the time-optimal solutions, the programmable-deviation controller has several advantages. They include smaller output voltage deviation during transients, lower current stress an implementation with much simpler hardware not requiring complex computations, and a high sampling rate analog-to-digital converter. These advantages allow for a significant reduction of reactive components of the converter and result in a lower current stress on the semiconductor switches. It should be noted that the operation of the controller has been demonstrated for cases of consecutive transients, which is the main job function for indirect energy transfer converters. The issue of nested transients is a topic for further research and will be addressed in future publications.

In steady state, the controller operates as a simple PCPM output voltage regulator. During transients, the controller sets the boundaries for the inductor current and the output voltage, such that the near minimum voltage deviation for a predetermined frequency range is obtained and that the convergence toward the new steady-state condition is ensured. The boundaries are set based on the founding that, in the case of a boost converter, the theoretical/ideal minimum deviation requires the boundary current to be equal to its new steady-state value and the boundary voltage equal to its minimum deviation. For that case, the converter recovers to the new steady state operating at the infinite switching frequency. To limit the switching frequency, the analysis of the relation of the minimum voltage boundary value for the frequency constrained case is performed and accordingly used in the control algorithm.

The effectiveness of the introduced controller is experimentally verified, through comparisons with the time optimal and conventional PCMP solutions. The results confirm that this modification of the PCMP architecture results in significantly better transient performance than the other solutions while eliminating the need for a high sampling rate ADC and complex computations.

Appendix A
Current Threshold-Based Programmable-Deviation Control Scheme

The programmable voltage deviation control method that is introduced in this paper provides both theoretical and practical insights into the load transient behavior of indirect energy transfer converters. The theoretical analysis has established the relationship between the converter state variables and a criterion to guarantee convergence toward the steady state has been defined. As a consequence, the control task of recovery from a load transient has been significantly simplified and reduced to realization of two comparators, one for each state variable (transient suppression logic block). Furthermore, within the defined boundaries, the concept allows independence in the selection of the current and voltage thresholds. This may assist in further research and improvement of the controller.

On the other hand, the preliminary concept as described in Section III may result in inconsistent performance due to parameters uncertainties. The values of *L* and *C* may vary and the input voltage is not constant in a number of applications. These factors can affect the accuracy of threshold calculations and

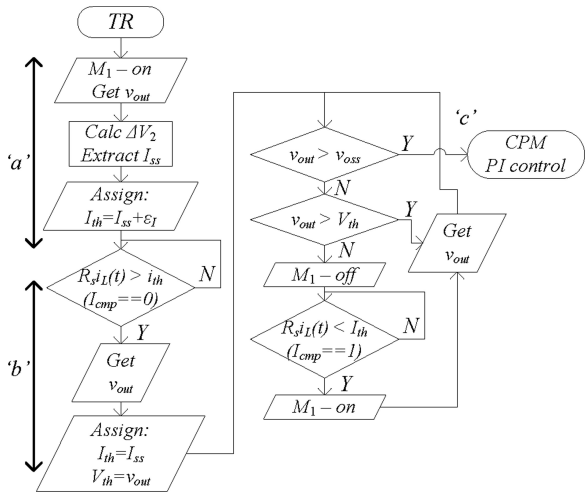

Fig. 19. Flowchart of the current threshold based transient suppression algorithm.

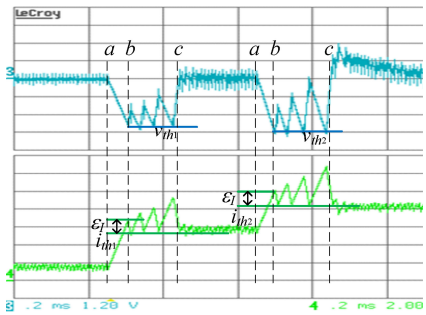

Fig. 20. Experimental demonstration of the current threshold-based programmable-deviation control for two consecutive light-to-heavy load transients (25 W–90 W–140 W). The additional charging current ε_I (for both steps) has been set to 15% of the first load step.

performance of the programmable-deviation controller. Therefore, it would be highly advantageous if the threshold settings could be extracted based on the new load current only, eliminating uncertainties that may appear in the system.

A possible solution of this problem is an alternative realization of the self-tuning estimator unit for thresholds calculations, which its operation is described with a help of the flowchart shown in Fig. 19 and experimentally demonstrated in Fig. 20 (a zoomed in version of Fig. 18). The operation principle of the controller is similar to its precursor (described in Section II), with the exception that upon detection of the transient and estimation of the new load current (point "*a,*" Figs. 19 and 20), the first on interval of the transistor is controlled by the current threshold such that (1) is satisfied, i.e., the inductor current is slightly larger than its new steady-state value $I_{\rm th} = I_{ss} + \varepsilon_I$. The value of ε_I can is either selected as a function of the current difference, or using (5) or (11). It should be noted that notation of ε_I refers to the additional charging current above I_{ss} as described in (1).

Once the first current threshold has been reached (point "*b,*" Figs. 19 and 20), the controller measures the output voltage and assigns $V_{\rm th} = V_{\rm out(point\,"b")}$ and $I_{\rm th} = I_{ss}$. From this point and on, the voltage is recovered using the transient suppression logic as described earlier. At the instance that the output voltage has reached its new steady-state value (point "*c,*" Figs. 19 and 20), the controllers resumes regular CPM operation.

Using this alternative approach, the thresholds settings become depended on the new load current only eliminating system uncertainties.

Appendix B
Peak Inductor Current Estimation

As can be observed throughout the paper, the peak inductor current in each cycle during light-to-heavy transient recovery is higher than its previous one. Estimation of the maximum inductor current during a transient period may be beneficial for the selection of the system components. This estimation can be facilitated by geometrical calculation of the state plane for the specified path of the final off cycle (point "*f*" to point "*o,*" Fig. 3). A generic off trajectory of a boost converter can be expressed as [10], [11], [32], [34]

$$C\left(v_c - V_{\rm in}\right)^2 + L\left(i_L - I_{\rm out}\right)^2 = C\left(v_{c0} - V_{\rm in}\right)^2 + L\left(i_{L0} - I_{\rm out}\right)^2. \quad (20)$$

By assigning $v_c = V_{\rm th}, i_L = I_{\rm max}, v_{c0} = V_{\rm out}, i_{L0} = I_{\rm out}/D'_{\rm oss}$, and after some manipulations, the peak inductor value can be estimated as follows:

$$I_{\rm max} = I_{\rm out} + \sqrt{\frac{C}{L}\left[\left(V_{\rm out} - V_{\rm in}\right)^2 - \left(V_{\rm th} - V_{\rm in}\right)^2\right] + \left(\frac{I_{\rm out}}{D'_{\rm oss}} - I_{\rm out}\right)^2}. \quad (21)$$

References

[1] Y. Qiu, J. Sun, M. Xu, K. Lee, and F. C. Lee, "Bandwidth improvements for peak-current controlled voltage regulators," *IEEE Trans. Power Electron.*, vol. 22, no. 4, pp. 1253–1260, Jul. 2007.

[2] W. Pit-Leong, F. C. Lee, Z. Xunwei, and C. Jiabin, "VRM transient study and output filter design for future processors," in *Proc. IEEE Ind. Electron. Soc. Conf.*, Aachen, Germany, 1998, vol. 1, pp. 410–415.

[3] N. Keskar and G. A. Rincon-Mora, "Self-stabilizing, integrated, hysteretic boost DC-DC converter," in *Proc. IEEE Ind. Electron. Soc. Annu. Conf.*, 2004, vol. 1, pp. 586–591.

[4] Z. Xunwei, X. Peng, and F. C. Lee, "A novel current-sharing control technique for low-voltage high-current voltage regulator module applications," *IEEE Trans. Power Electron.*, vol. 15, no. 6, pp. 1153–1162, Nov. 2000.

[5] Y. Panvo and M. M. Jovanović, "Design consideration for 12-V/1.5-V, 50-A voltage regulator modules," *IEEE Trans. Power Electron.*, vol. 16, no. 6, pp. 776–783, Nov. 2001.

[6] P. Midya, P. T. Krein, and M. F. Greuel, "Sensorless current mode control-an observer-based technique for DC-DC converters," *IEEE Trans. Power Electron.*, vol. 16, no. 4, pp. 522–526, Jul. 2001.

[7] Z. Lukic, N. Rahman, and A. Prodić, "Multi-bit Σ-Δ PWM digital controller IC for DC–DC converters operating at switching frequencies beyond 10 MHz," *IEEE Trans. Power Electron.*, vol. 22, no. 5, pp. 1693–1707, Sep. 2007.

[8] S. Saggini, P. Mattavelli, G. Garcea, and M. Ghioni, "A mixed-signal synchronous/asynchronous control for high-frequency DC-DC boost converters," *IEEE Trans. Power Electron.*, vol. 55, no. 5, pp. 2053–2060, May 2008.

[9] B. Patella, A. Prodić, A. Zirger, and D. Maksimović, "High-frequency digital PWM controller IC for DC/DC converters," *IEEE Trans. Power Electron*, vol. 18, no. 1, pp. 438–446, Jan. 2003.

[10] W. W. Burns and T. G. Wilson, "State trajectories used to observe and control dc-to-dc converters," *IEEE Trans. Aerosp. Electron. Syst.*, vol. AES-12, no. 6, pp. 706–717, Nov. 1976.
[11] W. W. Burns and T. G. Wilson, "A State-trajectory control law for dc-to-dc converters," *IEEE Trans. Aerosp. Electron. Syst.*, vol. AES-14, no. 1, pp. 2–20, Jan. 1978.
[12] V. Yousefzadeh, A. Babazadeh, B. Ramachandran, E. Alarcon, L. Pao, and D. Maksimović, "Proximate time-optimal digital control for synchronous buck DC-DC converters," *IEEE Trans. Power Electron.*, vol. 23, no. 4, pp. 2018–2026, Jul. 2008.
[13] A. Babazadeh and D. Maksimović, "Hybrid digital adaptive control for fast transient response in synchronous buck DC–DC converters," *IEEE Trans. Power Electron.*, vol. 24, no. 11, pp. 2625–2638, Nov. 2009.
[14] G. Feng, E. Meyer, and Y.-F. Liu, "A new digital control algorithm to achieve optimal dynamic performance in dc-to-dc converters," *IEEE Trans. Power Electron.*, vol. 22, no. 4, pp. 1489–1498, Jul. 2007.
[15] E. Meyer, Z. Zhang, and Y.-F. Liu, "An optimal control method for buck converters using a practical capacitor charge balance technique," *IEEE Trans. Power Electron.*, vol. 23, no. 4, pp. 1802–1812, Jul. 2008.
[16] W. Fang, Y.-J. Qiu, X.-D. Liu, and Y.-F. Liu, "A new digital capacitor charge balance control algorithm for boost DC/DC converter," in *Proc. IEEE Energy Conv. Cong. Expo.*, Sep. 2010, pp. 2035–2040.
[17] G. E. Pitel and P. T. Krein, "Minimum-Time transient recovery for DC–DC converters using raster control surfaces," *IEEE Trans. Power Electron.*, vol. 24, no. 12, pp. 2692–2703, Dec. 2009.
[18] P. S. Shenoy, P. T. Krein, and S. Kapat, "Beyond time-optimality: Energy-based control of augmented buck converters for near ideal load transient response," in *Proc. IEEE Appl. Power Electron. Conf. Expo.*, Mar. 2011, pp. 916–922.
[19] M. Ordonez, M. T. Iqbal, and J. E. Quaicoe, "Selection of a curved switching surface for buck converters," *IEEE Trans. Power Electron.*, vol. 21, no. 4, pp. 1148–1153, Jul. 2006.
[20] A. Radic, Z. Lukic, A. Prodić, and R. de Nie, "Minimum deviation digital controller IC for single and two phase dc-dc switch-mode power supplies," *IEEE Tran. Power Electron.*, vol. 28, no. 9, pp. 4281–4298, Sep. 2013.
[21] Z. Lukić, S. M. Ahsanuzzaman, Z. Zhao, and A. Prodić, "Sensorless self-tuning digital CPM controller with multiple parameter estimation and thermal stress equalization," *IEEE Tran. Power Electron.*, vol. 26, no. 12, pp. 3948–3963, Dec. 2011.
[22] S. Kapat, A. Patra, and S. Banerjee, "A novel current controlled tristate boost converter with superior dynamic performance," in *Proc. IEEE Int. Symp. Circuit Syst.*, 2008, pp. 2194–2197.
[23] O. Trescases, N. Rahman, A. Prodić, and W.-T. Ng, "A 1V buck converter IC with hybrid current-mode control and a charge-pump DAC," in *Proc. IEEE Power Electron. Spec. Conf.*, Jun. 2008, pp. 1122–1128.
[24] K. I. Hwu and Y. T. Yau, "Improvement of the unloading transient response for the PFM-controlled buck-type converter," in *Proc. IEEE Region 10 Conf.*, 2006, pp. 1–4.
[25] O. Trescases, N. Rahman, W.-T. Ng, and A. Prodić, "A low-power mixed-signal current-mode DC-DC converter using a one-bit $\Delta\Sigma$ DAC," in *Proc. IEEE Appl. Power Electron. Conf. Expo.*, Mar. 2010, pp. 700–704.
[26] G. Garcea, P. Mattavelli, K. Lee, and F. C. Lee, "A mixed-signal control for VRM applications," in *Proc. Eur. Conf. Power Electron. Appl.*, 2005, pp. 1–10.
[27] G. Rahav and S. Ben-Yaakov, "Forbidden state space trajectories of PWM converters: Implication to digital control," in *Proc. IEEE Power Electron. Spec. Conf.*, Jun. 1999, pp. 1199–1203.
[28] M. M. Peretz, "Hybrid control method for optimal transient response and output filter minimization for buck-boost type converters," in *Proc. Int. Exhib. Conf. Power Electron.*, Nuremberg, Germany, 2013.
[29] R. Venkataramanan, "Sliding mode control of power converters," Ph.D. dissertation, California Inst. Technol., Pasadena, CA, USA, May 1986.
[30] E. Santi, D. Li, A. Monti, and A. M. Stankovic, "A geometric approach to large-signal stability of switching converters under sliding mode control and synergetic control," in *Proc. IEEE Power Electron. Spec. Conf.*, Jun. 2005, pp. 1389–1395.
[31] R. Munzert and P. T. Krein, "Issues in boundary control," in *Proc. IEEE Power Electron. Spec. Conf.*, Jun. 1996, pp. 810–816.
[32] M. Greuel, R. Muyshondt, and P. T. Krein, "Design approaches to boundary controllers," in *Proc. IEEE Power Electron. Spec. Conf.*, Jun. 1997, pp. 672–678.
[33] T.-T. Song and H. S Chung, "Boundary control of boost converters using state-energy plane," *IEEE Trans. Power Electron.*, vol. 23, no. 2, pp. 551–563, Mar. 2008.
[34] J. M. Galvez, M. Ordonez, F. Luchino, and J. E. Quaicoe, "Improvements in boundary control of boost converters using the natural switching surface," *IEEE Trans. Power Electron.*, vol. 26, no. 11, pp. 3367–3376, Nov. 2011.
[35] A. Prodić, J. Chen, R. W. Erickson, and D. Maksimović, "Digitally controlled PFC rectifier having fast dynamic response," in *Proc. IEEE Appl. Power Electron. Conf.*, Mar. 2002, pp. 476–482.
[36] A. Prodić, R. W. Erickson, and D. Maksimović, "Dead-zone digital controllers for wide-bandwidth voltage loop of PFC regulators," *IEEE Trans. Power Electron.*, vol. 21, no. 1, pp. 173–181, Jan. 2006.
[37] DE2 Development and Education Board user manual, Altera Corporation, San Jose, CA, USA, 2006.
[38] Spartan-3A DSP FPGA Family Data Sheet, Xilinx Corporation, DS610, Oct. 4, 2010.
[39] TMS320F2801–60 Data Manual, Texas Instruments Inc., SPRS230N, May 2012.
[40] dsPIC33EPXXXGP50X 16-Bit Microcontrollers and Digital Signal Controllers with High-Speed PWM, Microchip Technology Inc., DS70000657H, 2013.

Mor Mordechai Peretz (S'05–M'12) was born in Beer-Sheva, Israel, in 1979. He received the B.Tech. degree in electrical engineering, in 2003, from the Negev Academic College of Engineering, Beer-Sheva, and the M.Sc. and Ph.D. degrees in electrical and computer engineering from Ben-Gurion University of the Negev, Negev, Israel, in 2005 and 2010, respectively.

From 2010 to 2012, he was a Postdoctorate Fellow at the Laboratory for Low-Power Management and Integrated Switch-Mode Power Supplies (SMPS), University of Toronto, Canada. In 2012, he joined the Department of Electrical and Computer Engineering in Ben-Gurion University, and is currently the Director of the Power Electronics Laboratory there. His research interests include digital and smart control methods for efficient-energy processing, SMPS miniaturization, mixed-signal IC design of SMPS, modeling and computer aided design, applications of nonlinear magnetics, and renewable energy systems.

Behzad Mahdavikhah (S'11) received the B.Sc. degree in electrical engineering from Sharif University of Technology, Tehran, Iran, and the M.A.Sc. degree in electrical engineering from McMaster University, Hamilton, ON, Canada, in 2007 and 2009, respectively. He is currently working toward the Ph.D. degree in electrical engineering, University of Toronto, ON, Canada.

Since September 2009, he has been a Research Assistant at the Laboratory for Power Management and Switch-Mode Power Supplies, University of Toronto. His research interests include converter topologies, digital control techniques, and mixed-signal IC design for high-frequency switch-mode power supplies.

Aleksandar Prodić (S'00–M'03) received the Dipl.Ing. degree in electrical engineering from the University of Novi Sad, Novi Sad, Serbia, in 1994, and the M.Sc. and Ph.D. degrees from the Colorado Power Electronics Center, University of Colorado, Boulder, CO, USA, in 2000 and 2003, respectively.

In 2003, he joined the University of Toronto, Toronto, ON, Canada, where he established the Laboratory for Power Management and Integrated Switch-Mode Power Supplies (SMPS) in 2004 and is currently an Associate Professor with the Department of Electrical and Computer Engineering. His research interests include practical advanced control methods for power electronics, converter topologies, mixed-signal IC design for power electronics, low-power high-frequency SMPS, and power management systems. The applications of interest range from on-chip power supplies for portable devices to power management systems in hybrid and electric vehicles. His research also covers use of power electronics in biomedical applications.